World Journal of Pharmaceutical Science and Research
www.wjpsronline.com
Research Article
ISSN: 2583-6579
SJIF Impact Factor: 6.916
Year - 2026
Volume: 5; Issue: 5
Page: 16-35

ADAMANTANE AMINE DERIVATIVES AS MULTITARGET COMPOUNDS FOR ALZHEIMER'S DISEASE: *IN SILICO*, *IN VITRO*, AND *IN VIVO* STUDIES

Adriana Garcia*[1,2], Mauro V. de Almeida[2], Hélio F. Dos Santos[2], José M. S. de Campos[3†], Heveline Silva[4], Aline F. da Silva[5], Felix A. A. Soares[5], Nádia R. B. Raposo[1]

[1]NUPICS, Faculdade de Farmácia, Universidade Federal de Juiz de Fora, Juiz de Fora, MG, 36036-900, Brazil.
[2]Departamento de Química, Universidade Federal de Juiz de Fora, Juiz de Fora, MG, 36036-900, Brazil.
[3]Departamento de Biologia, Instituto de Ciências Biológicas, Universidade Federal de Juiz de Fora, Juiz de Fora, MG, Brazil. †Deceased prior to publication
[4] Departamento de Química, Universidade Federal de Minas Gerais, Belo Horizonte, MG, 31270-901, Brazil.
[5]Departamento de Bioquímica e Biologia Molecular, Universidade Federal de Santa Maria, Santa Maria CEP, RS 97105-900, Brazil.

Article Received: 05 March 2026 | | ***Article Revised: 27 March 2026*** | | ***Article Accepted: 16 April 2026***

***Corresponding Author: Adriana Garcia**
NUPICS, Faculdade de Farmácia, Universidade Federal de Juiz de Fora, Juiz de Fora, MG, 36036-900, Brazil.
DOI: https://doi.org/10.5281/zenodo.19910419

How to cite this Article: Adriana Garcia, Mauro V. de Almeida, Hélio F. Dos Santos, José M. S. de Campos, Heveline Silva, Aline F. da Silva, Felix A. A. Soares, Nádia R. B. Raposo (2026) ADAMANTANE AMINE DERIVATIVES AS MULTITARGET COMPOUNDS FOR ALZHEIMER'S DISEASE: IN SILICO, IN VITRO, AND IN VIVO STUDIES. World Journal of Pharmaceutical Science and Research, 5(5), 16-35.

ABSTRACT

Adamantoid amino compounds were investigated for their effects on two primary targets in Alzheimer's disease, acetylcholinesterase (AChE) and NMDA receptor. The compounds were synthesized in two steps: the hydroxyl group of adamantane-1-methanol was substituted with iodine, followed by replacement with an amine. Compounds were tested as acetylcholinesterase inhibitors (iAChE - Ellman test) and antioxidant activity against 2,2-diphenyl-1-picrylhydrazyl (DPPH). Toxicity was evaluated employing the *Artemia salina* and *Allium cepa* assays. Cytotoxicity was determined in glial cells (U87) and mouse fibroblasts (L929) by the MTT test. Compounds exhibited high AChE inhibition capacity (78-97%) and low antioxidant activity (less than 35%). The samples had different cytotoxic performances. Compounds **1**, **2**, **3**, and **5**, which had a terminal NH_2 group, were more cytotoxic than the samples with this group replaced, reinforcing its importance for biological activity. This pattern was also observed in the iAChE test and confirmed by molecular docking studies. Compound **3** was the most promising, exhibiting higher enzyme inhibition (iAChE, 97%) and no toxic effects in the *Artemia salina* assay. The *C elegans* trial confirmed the ability of compound **3** to act on different therapeutic targets, modulating the cholinergic and glutamatergic activity in the pharyngeal beat test and locomotor parameters of the nematode.

KEYWORDS: Alzheimer's disease; Cholinesterase inhibitors; Molecular Docking; NMDA receptor; *Caenorhabditis elegans.*

INTRODUCTION

Alzheimer's disease (AD) is the most prevalent chronic neurodegenerative disease leading to dementia. It is a multifactorial, progressive, degenerative brain disorder that initially affects the areas of the brain responsible for memory, thought, and language, resulting posteriorly in a decline in overall cognitive function. Alzheimer's has become a significant public health concern due to rising global life expectancy.[1,2,3]

Nowadays, there is no blockbuster drug to delay the course of the disease. The pharmacological treatment is based on cholinesterase inhibitors (the increase of acetylcholine levels in the brain improves cognitive function) and memantine (a modulator of glutamate activity, that protects neurons from glutamate-induced excitotoxicity). These drugs attenuate cognitive deterioration to a modest extent, have relatively few side effects, and have good evidence of long-term outcomes.[4,5]

Cutting-edge research continues to investigate innovative treatments, such as disease-modifying treatments like amyloid-*β*-targeting antibodies. However, these immunotherapies targeting amyloid plaques or tau tangles show modest efficacy in reducing disease progression, are associated with significant side effects, have limited data regarding long-term outcomes, and are extremely expensive[6] Current therapies fail to adequately address the multifactorial nature of AD. Multi-Target Directed Ligands (MTDLs) are drugs designed to interact with multiple pathological targets involved in the fundamental mechanisms of AD. This approach relies on the ability of a single molecule to modulate distinct biological pathways, each contributing to the complex pathophysiology of the disease, and eliciting diverse pharmacological effects. An additional advantage of MTDLs is the potential to reduce the need for polypharmacy, which is particularly beneficial for patients who, at more advanced stages of AD, often face significant challenges with medication adherence. Therefore, the development of MTDLs represents a promising strategy to improve therapeutic efficacy while minimizing treatment complexity in AD.[7]

MATERIALS AND METHODS

All reagents and solvents were used without further purification. Infrared (IR) spectra were recorded on a BRUKER ALPHA ATR (*Attenuated Total Reflectance - diamond*) Spectrometer, in the region of 4000–400 cm^{-1}, with a spectral resolution of 4 cm^{-1}, and an average of 64 scans. ^{1}H NMR (500 MHz) and ^{13}C NMR (125 MHz) spectra were recorded in methanol-*d4* or dimethyl sulfoxide-*d6* (DMSO) solvents on a BRUKER AVANCE III HD 500 MHz spectrometer, the chemical shifts were expressed in the δ scale (ppm), in line with previous reports.[8]

Synthesis of adamantane amine derivatives (Scheme 1)

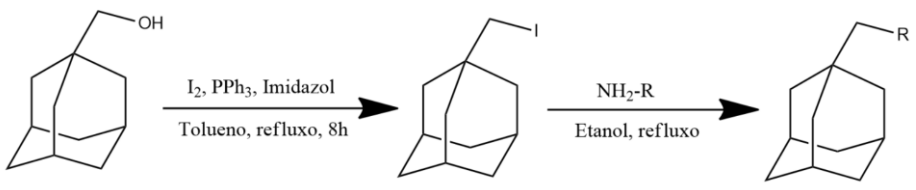

Scheme 1: Synthetic pathway of the adamantane amine derivatives.

Compounds were prepared from 1-adamantanemethanol as described in the literature.[9] The alcohol was treated initially with triphenylphosphine, imidazole, and iodine in toluene for 24 h at 90 °C. The replacement of iodine in 1-adamantanemethyl iodide was achieved by reaction with the selected amine in ethanol (see Scheme 1) at reflux.[10]

The amines used were 1,2-ethylenediamine; 1,3-propanediamine; 1,4-butanediamine; N^1,N^1-dimethylethane-1,2-diamine; 2-aminoethanethiol and piperazine (Fig. 1). After purification by column chromatography, the compound was dissolved in methanol and converted into its hydrochloride salt by acidification to pH 2.0 with hydrochloric acid. The precipitated solid was collected by filtration after standing at room temperature.

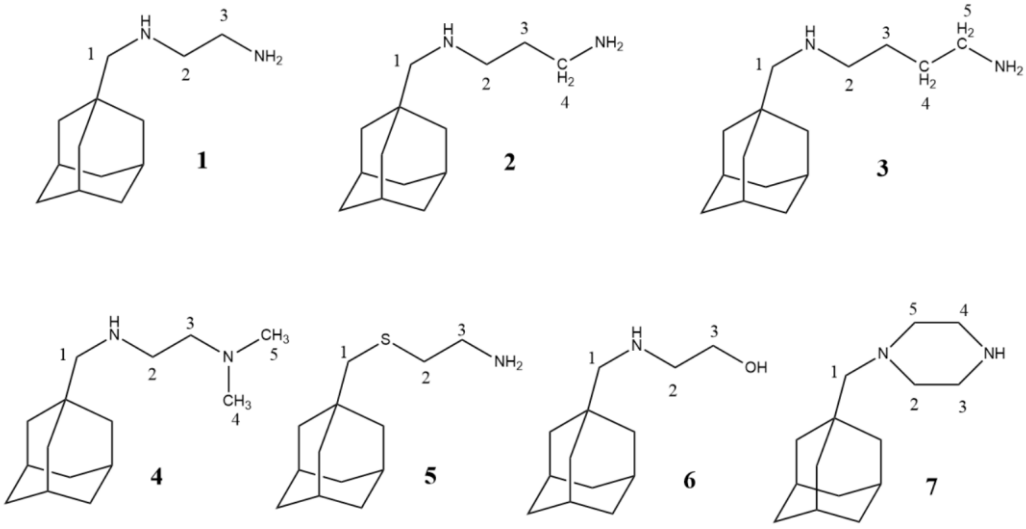

Fig. 1: Structure of compounds 1-7 *(the numbering used is not based on IUPAC nomenclature and is only to facilitate the identification of atoms in the characterization).*

1 - [N^1-((3r,5r,7r)-Adamantan-1-ylmethyl)ethane-1,2-diamine] dihydrochloride

IR ν_{max} (cm^{-1}): 3380, 2898, 2846, 1444. ^{1}H NMR [500 MHz, CD_3OD, δ (ppm)]: 1.6 – 2.0 (m, 15H, H-adamantyl); 2.8 (s, 2H, H1); 3.3 – 3.4 (m, 4H, H2 and H3). ^{13}C NMR [125 MHz, CD_3OD, δ (ppm)]: 29.5; 33.6; 37.6; 40.9 (C-adamantyl); 36.9 (C3) 47.2 (C2); 61.5 (C1).

2 - [N^1-((3r,5r,7r)-Adamantan-1-ylmethyl)propane-1,3-diamine] dihydrochloride

IR ν_{max} (cm^{-1}): 3355, 2902, 2846, 1444. ^{1}H NMR [500 MHz, CD_3OD, δ (ppm)]: 1.6 – 2.0 (m, 15H, H-adamantyl); 2.1-2.3 (m, 2H, H3); 2.7 (s, 2H, H1); 3.0 – 3.1 (m, 4H, H2 and H4). ^{13}C NMR [125 MHz, CD_3OD, δ (ppm)]: 25.0 (C3); 29.5; 33.5; 37.5; 40.8 (C-adamantyl); 38.1 (C4); 47.4 (C2); 61.0 (C1).

3 - [N^1-((3r,5r,7r)-Adamantan-1-ylmethyl)butane-1,4-diamine] dihydrochloride

IR ν_{max} (cm^{-1}): 3467, 3402 2900, 2846, 1448. ^{1}H NMR [500 MHz, CD_3OD, δ (ppm)]: 1.6 – 2.0 (m, 19H, 15H-adamantyl; 4H, H3, H4); 2.7 (s, 2H, H1); 3.0 (m, 2H, H2); 3.3 (m, 2H, H5); ^{13}C NMR [125 MHz, $(CD_3)_2SO$, δ (ppm)]: 21.6 (C3); 23.9 (C4); 27.3; 31.8; 35.9 (C-adamantyl); 37.9 (C5) 47.3 (C2); 58.0 (C1).

4- [N^1-((3r,5r,7r)-Adamantan-1-ylmethyl)-N^2,N^2-dimethylethane-1,2-diamine] dihydrochloride

IR ν_{max} (cm^{-1}): 3400, 2902, 2848, 1461. ^{1}H NMR [500 MHz, CD_3OD, δ (ppm)]: 1.7 – 2.0 (m, 15H, H-adamantyl); 2.8 (s, 2H, H1); 3.0 (m, 6H, H4 and H5); 3.5 (m, 4H, H2 and H3). ^{13}C NMR [125 MHz, CD_3OD, δ (ppm)]: 29.3; 33.5; 37.4; 40.8 (C-adamantyl); 43.9 (C4 and C5); 44.7 (C2); 54.4 (C3) 61.5 (C1).

5 - [2-(((3r,5r,7r)-A damantan-1-ylmethyl)thio)ethanamine] hydrochloride

IR ν_{max} (cm^{-1}): 3425, 2898, 2842, 1454, 881, 813. ^{1}H NMR [500 MHz, $(CD_3)_2SO$, δ (ppm)]: 1.5 – 1.9 (m, 15H, H-adamantyl); 2.3 (s, 2H, H1); 2.7 (2H, H2); 2.9 (m, 2H, H3); 8.1 (s, 3H, NH_2.HCl). ^{13}C NMR [125 MHz, $(CD_3)_2SO$, δ (ppm)]: 27.8; 33.4; 36.3; 41.0 (C-adamantyl); 30.1 (C2); 38.7 (C1); 46.1 (C3).

6 - [2-(((3r,5r,7r)-Adamantan-1-ylmethyl)amino)ethanol] hydrochloride

IR ν_{max} (cm^{-1}): 3349, 2904, 2848, 1442, 1080. ^{1}H NMR [500 MHz, CD_3OD, δ (ppm)]: 1.6 – 2.0 (m, 15H, H-adamantyl); 2.8 (s, 2H, H1); 3.1 (m, 2H, H2); 3.8 (m, 2H, H3). ^{13}C NMR [125 MHz, CD_3OD, δ (ppm)]: 28.0; 32.0; 36.0; 39.1 (C-adamantyl); 50.1 (C2); 55.6 (C3); 58.6 (C1).

7 - [1-((3r,5r,7r)-Adamantan-1-ylmethyl)piperazine] dihydrochloride

IR ν_{max} (cm^{-1}): 3295, 2906, 2850, 1442, 1421, 1353. ^{1}H NMR [500 MHz, CD_3OD, δ (ppm)]: 1.7 – 2.0 (m, 15H, H-adamantyl); 3.0 (s, 2H, H1); 3.4 – 3.9 (m, 8H, piperazine). ^{13}C NMR [125 MHz, CD_3OD, δ (ppm)]: 28.3; 33.3; 35.8; 39.2 (C-adamantyl); 39.8 (C3); 51.5 (C2); 70.0 (C1).

***In vitro* AChE inhibitory assay**

The acetylcholinesterase inhibition test followed the methodology described by Ellmam with adaptations.[11] It was performed in a microplate, to which different concentrations of the compounds to be tested were added in Tris-HCl buffer, 50 mM, pH 8.0. In 96-well plates, were added 25 µL of 15 mM AChI in water, 125 µL of 3 mM dithiobisnitrobenzoic acid (DTNB), 50 µL of the buffer, and 25 µL of the tested molecules dissolved in MeOH at concentrations ranging from 62.5 to 1000 $\mu g.mL^{-1}$. Then, 25 µL of AChE solution (0.22 U mL^{-1}) was added, and the absorbance measured in a spectrophotometer (SpectraMax 190, Molecular Devices, Sunnyvale, CA, USA) at a wavelength of 415 nm at 15-second intervals and 41 cycles at 37 °C. All assays were performed in triplicate. The percentage of inhibition was calculated using the following equation:

$$\%Inhibition = [(E - S)/S] \times 100$$

where E is the enzyme activity without the test compound, and S is the enzyme activity with the tested compound. IC_{50} was determined by nonlinear regression in Graph Pad Prism version 6.0 for Windows, Graph Pad Software (San Diego, CA, USA), and represents the concentration capable of inhibiting 50% of the hydrolysis of acetylcholine.

Antioxidant activity

Antioxidant activity was measured by 2,2-diphenyl-1-picrylhydrazyl (DPPH) free radical method[12] with minor modifications. Briefly, different concentrations of the sample (50 µL; 0.97–250 $\mu g.mL^{-1}$) in methanol were added to each well of a 96-well microplate and mixed with 150 µL of 50 µM DPPH in ethanol solution. The reaction was kept in the dark for 30 min at room temperature. Then, absorbance was measured in a spectrophotometer at 510 nm against the negative control (ethanol). To obtain the % inhibition of DPPH, we used the equation:

$$IC_{50}\ (\%) = 100 \times (A0 - As) / A0,$$

where A0 is the absorbance of the negative control and As is the absorbance of the test sample. The IC_{50} was calculated from the linear equation of the linear scatter plot and represents the concentration that inhibits 50% of the DPPH radical. All tests were in triplicate.

Cytotoxicity assay

To determine cell viability, the cell lines used were L929 (mouse fibroblasts) and U87 (human glioblastoma cells). L929 cells were distributed in RPMI 1640 culture medium, supplemented with 10% v/v fetal bovine serum (FBS), being 1 x 10^3 cells/well/100 µL in 96-well plates that were incubated at 37 °C in a humidified atmosphere at 5% CO_2 for 24 hours for total adhesion. U87 cells were distributed in DMEM culture medium supplemented with sodium pyruvate (1% v/v) and fetal bovine serum (FBS) 10% v/v at 3 x 10^3 cells/well/100 µL in 96-well plates that were incubated at 37 °C in a humidified atmosphere at 5% CO_2 for 24 hours for total adhesion. In the wells of the plate containing the already adhered cells, 100 µL of decreasing concentrations (100, 10, 1, 0.1, and 0.01 µM) of the substance tested were distributed in quadruplicates. The stock solutions were prepared in DMSO and diluted in a culture medium (maximum of 1% v/v DMSO). For negative control, 100 µL of supplemented culture medium. After 72 hours of exposure to the compounds, the cells were incubated with MTT (5 µg/10 µL/well) for four hours. Then, all supernatant liquid was aspirated, 100 µL of DMSO/well added, and cell viability (proportional to the concentration of formazan salts – a product of mitochondrial reduction of MTT in viable cells) was determined by measuring absorbance at 570 nm in a microplate spectrophotometer [13]. Data obtained through cytotoxic assays were normalized considering the cell viability of the negative control as 100% using GraphPad Prism 8.0 software.

Acute toxicity with *Artemia salina*

The brine shrimp lethality assay was carried out following the procedure described by Meyer with some modifications.[14] Encysted eggs of *Artemia salina* were incubated in artificial seawater (48 hours; room temperature). After this time, ten nauplii were placed in each well, with the sample (10 – 1,000 µg.mL^{-1}) dissolved in 0.1% DMSO added. The final volume (5 mL) was completed with saline. Thymol was used as the positive control, and DMSO 0.1% was the negative control. After 24 hours, the number of survivors was counted, and the percentage of lethality was calculated using Abbott's equation. The lethal concentration of 50% (LC_{50}) was calculated by Probit analysis.[15]

$$\% \text{ mortality} = [1 - (\text{n° alive treatment} / \text{n° alive control})] \times 100.$$

Citogenotoxicity in *Allium cepa*

Root tips were pretreated with five concentrations of compound **3** for 24 hours at 10 °C, then fixed in absolute ethanol/glacial acetic acid (3:1, v/v) at room temperature for another 24 hours and subsequently stored at −20 °C until analysis. Fixed root tips were washed in 10 mM citrate buffer, pH 4.6, and digested in a solution of 4% cellulase, 1% pectolyase, and 4% hemicellulase at 37 °C for approximately 30 minutes. Digested root tips were macerated in a drop of 45% acetic acid, and slides were covered with coverslips. The coverslips were then removed in liquid nitrogen, after which the slides were air-dried and subsequently stained. The assay was performed in quadruplicate.[16] The concentrations tested were selected based on the IC_{50} values obtained from the acetylcholinesterase inhibition assay for compound **3** (0.21 mM). For convenience, the concentrations are hereafter to as 0.2x (0.042 mM), 0.5x (0.105 mM), 1x (0.21 mM), 2x (0.42 mM) and 5x (1.05 mM).

Docking simulation

Docking simulation was performed for all compounds in Figure 1. The 3D structures of all ligands tested were optimized at AM1 semiempirical level of theory using the Gaussian 09 program.[17] The 6U37 PDB structure was used for AchE,[18] which contains an o-ethylmethylphosphonic acid ester group (VX) attached to Ser203, two molecules of glycerol (GOL) and the ligand (2E)-N-[2-(azepan-1-yl]ethyl]-2-(hydroxyimino) acetaminde (PVQ - an oxima that acts

as AChE reactivator). The structure was cleaned removing all non-standards residues and structural waters, keeping only the chain A. The grid box was defined using the PVQ ligand as reference, centered at x = -25.034, y = 90.926, z = -8.203 Å with search space of 30 Å and spacing 0.375 Å in all three directions. Only polar H atoms were considered for AChE with the residues in their standard protonation states at neutral pH. The simulations were made with the Autodock Vina v1.1.2 software,[19,20] setting exhaustiveness = 8.

Before docking the compounds (**Fig. 1**), the docking protocol was validated for the Food and Drug Administration (FDA) approved drugs donepezil (E20), (-) galantamine (GNT), (-) huperzine A (HUP) and rivastigmine (RIS) (**Fig. S1**). The best pose of each ligand was compared to the X-ray structure available in the PDB with codes 4EY7 (E20), 4EY6 (GNT) and 4EY5 (HUP).[21]

In vivo* studies with *C. elegans

C. elegans Maintenance and Exposure

The wild-type C. elegans strain (N2) were maintained on Nematode Growth Medium (NGM) plates at 20 °C. To obtain a synchronized population, gravid adult worms were collected and treated with a bleaching solution consisting of 1% sodium hypochlorite (NaOCl) and 0.25 mol·L^{-1} sodium hydroxide (NaOH), which lysed the adults and released the eggs. The eggs were incubated in M9 buffer in the absence of food for 16 to 24 h, resulting in synchronized L1 larvae.[22] Synchronized L1-stage larvae were exposed in liquid medium to a range of concentrations (1, 5, 10, 25, 50, and 100 μM) of the compound **3** or memantine hydrochloride for 1h. Each treatment was performed in sterile 1.5 mL microcentrifuge tubes containing approximately 250–300 nematodes in a final volume of 1 mL. Following exposure, worms were assigned to either acute or chronic exposure groups. For the chronic exposure group, approximately 100 worms were immediately transferred to fresh NGM plates seeded with OP50 and incubated at 20 °C until behavioral assays were performed. For the acute exposure group, worms were washed three times with M9 buffer to remove any residual compound, then transferred to seeded NGM plates and maintained under the same conditions.

Survival assay

Following the incubation period, approximately 100 animals per group per experiment were observed under an optical microscope (Olympus model SZ2-LGB) and scored as alive or dead after failing to respond to mechanical stimuli. Three independent experiments were performed.[22]

Pharyngeal pumping

Using a microscope, the number of pharyngeal contractions of each worm on the treatment plate was counted for 10 s; the tests were run in triplicate. Subsequently, the values for each worm were averaged and expressed as the pharyngeal pumping/minute. Ten worms per group per experiment were evaluated in three independent experiments.[23]

Head Thrashes

Previously treated worms in the young adult stage were chosen at random and placed for 1 min in a drop of M9 buffer. Then, the number of head movements of each worm was counted for 20 s. Three independent experiments were performed, with 10 worms per group per experiment.[23]

Touch response

The touch response was evaluated by gently stimulating the head region of each worm with a fine bristle brush. A backward movement was considered a positive response. Worms that showed no reaction after ten consecutive touches were classified as non-responsive.[24]

Body Length and Locomotor Parameters by WormLab®

To evaluate body length and locomotor behavior, worms were transferred after 48 h of treatment to M9 buffer and recorded for 30 seconds using a stereomicroscope equipped with a digital camera. Videos were analyzed using WormLab software (MBF Bioscience, Williston, VT, USA). Body length was automatically measured based on the worm skeletonization function of the software. Additionally, locomotor parameters such as swimming speed, wave initiation rate, dynamic amplitude, and curling were extracted from the same recordings.[23] Three independent experiments were carried out, with at least 10 animals per group per experiment.

RESULTS AND DISCUSSION

Chemistry

Compounds (see **Fig.1**) were prepared from 1-adamantanemethanol (**Scheme 1**) as described in the literature[9,10] and characterized by NMR and infrared.

***In vitro* tests**

The seven compounds were classified as potent AChE inhibitors (> 50%) based on the Ellman method (Table 1).[25]

Antioxidant capacity was also evaluated, given the relevance of oxidative stress in AD and the brain's high susceptibility to oxidative damage due to its physiology and the restrictive nature of the blood-brain barrier, which protects the brain from toxins, also prevents/reduces the absorption of some antioxidants.[26]

All compounds inhibited AChE (78.4 to 97.4%), with **3** reaching 97.4% and an IC_{50} = 0.21 mM. Terminal NH_2 groups favored enzyme inhibition, while substitutions with $N(CH_3)_2$ (compound **4**), N-piperazine (compound **7**) or OH (compound **6**) reduced activity. Chain length influenced inhibition only for compound **3** (four carbons). Antioxidant capacity was low (19.9 to 34.2%), with no clear structure-activity relationship.

Table 1: Acetylcholinesterase inhibitory capacity and antioxidant activity.

	Molecular weight ($g.mol^{-1}$)	% Inhibition AChE	IC_{50} AchE (mM)	% DPPH Inhibition
1	281.26	92.5%	0.78	22.6%
2	295.29	91.5%	1.48	26.2%
3	309.32	97.4%	0.21	19.9%
4	309.32	85.5%	0.75	33.3%
5	261.85	91.5%	0.12	30.0%
6	245.79	78.4%	0.72	21.9%
7	307.30	87.6%	0.81	34.2%

All tests were performed in triplicate.

Cytotoxicity was then evaluated using L929 and U87 cell lines (Table 2). Compounds **4** and **6** were non-cytotoxic up to 100 μM in both cell lines. **5** and **7** showed moderate activity (approximately 40 μM). Compound **1** was more cytotoxic to L929 (39.2 ± 1.3 uM), while compounds **2** and **3** were significantly more toxic to U87 cells (10.6 ± 0.4 and 4.7 ± 0.1, respectively) and less toxic to L929 cells (32.7 ± 1.3 and 24.5 ± 0.6, respectively). Higher cytotoxicity was associated

with terminal NH_2 groups (compounds **1**, **2**, **3** and **5**), whereas compounds with tertiary amine or hydroxyl were less toxic (compounds **4** a **6** respectively). Increasing the carbon chain enhanced cytotoxicity, particularly in U87 cell, indicating potential selectivity.

Table 2: IC_{50} – Inhibitory concentration of 50% of cell viability.

	IC_{50} (µM ± SD)*	
	U87 cells	**L929 cells**
1	60.0 ± 1.0	39.2 ± 1.3
2	10.6 ± 0.4	32.7 ± 1.3
3	4.7 ± 0.1	24.5 ± 0.6
4	>100	>100
5	40.1 ± 1.8	36.6 ± 1.6
6	>100	>100
7	39.5 ± 0.4	36.9 ± 0.6

**IC_{50} is defined as the concentration of the drug required to inhibit 50 % cell growth. Data are shown as the mean value of two independent experiments performed in quadruplicate with the corresponding standard deviations (SD).*

Acute toxicity was assessed using the *Artemia salina* bioassay, with larvae exposed to different concentrations for 24 hours. Mortality rates and LC_{50} values were calculated (Table 3), with $LC_{50} < 1{,}000$ µg.mL^{-1} considered toxic.[14]

Despite structural similarities, the compounds showed varying toxicity. Only compounds **3** and **6** were not toxic. Compound **3**, synthesized from 1,4-butane-diamine, has the longest carbon chain (four CH_2 groups), while **2**, with slightly shorter chain (three CH_2 groups), was the most toxic, highlighting the impact of chain length on toxicity. Compound **6**, synthesized from 2-aminoethanol, contains a hydroxyl group instead of a primary amine, which reduced toxicity, but also lowered acetylcholinesterase inhibition.

Table 3: Lethal concentration (LC_{50}) that induces acute toxicity for *Artemia salina.*

Compounds	LC_{50} (µg.mL^{-1} ± SD*)
1	72.4 ± 4.3
2	12.5 ± 3.0
3	>1000
4	63.0 ± 5.4
5	57.5 ± 4.3
6	>1000
7	83.7 ± 4.2
Thymol	16.1 ± 3.0

All tests were performed in triplicate

**Mean ± SD (Standard deviation).*

Given compound **3**'s strong AChE inhibition, favorable cell viability, and lack of toxicity to *Artemia salina*, it was selected for the *Allium cepa* assay and *in vivo* assays with *C. elegans*. The *Allium cepa* assay assesses genotoxic effects on meristematic cells. Treatment with compound **3** at 0.5x concentration significantly increased mitotic index (MI, percentage of dividing cells) by two percentage points ($p<0.05$), whereas 2x and 5x concentrations caused a significant reduction – on average 3.34-fold compared to the negative control ($p<0.05$). The 1x concentration showed no significant difference. In the phase analysis the treatments with 0.2x, 0.5x, 2x, and 5x concentrations significantly increased the prophase index (IProf) ($p<0.05$), with increases of 1.14-; 1.19-; 1.22-; and 1.38-fold, respectively, compared to the negative control (distilled water). The 1x concentration showed no statistically significant difference

(p>0.05). For the metaphasic index (IMeta), only the 5x treatment presented a significant reduction of 4.52 percentage points compared to the negative control (p<0.05). The anaphase index (IAnaf) showed no significant diferences at any concentration. The telophase index (ITelo) demonstrated significant reductions at 0.2x, 2x, and 5x compared to the negative control (p<0.05).

The results for chromosomal alterations and micronuclei are in Table 4. Both aneugenic and clastogenic effects were observed, however statistically significant changes occurred at the 2x and 5x concentrations. These treatments led to an increased percentage of cells exhibiting chromosomal alterations and micronuclei (p<0.05). Although the frequency of aneugenic alterations was higher than that of clastogenic alterations at 5x concentration (7.24% *versus* 4.02%), both alterations showed a nearly identical increase relative to the negative control, with 2.25-fold increase in aneugenic alterations and 2.26-fold in clastogenic alterations (Table 4). Regarding micronuclei, there was an absolute increase of 2.70 percentage points compared to the control (p<0.05).

Table 4: Percentage of chromosomal alterations and micronuclei after 24 hours of exposure to compound 3.

Compound 3 concentrations	Aneugenic effect	Clastogenic effect	Micronucleus formation
Negative control	3.21[a]	1.78[a]	0.78[a]
0.2x	3.45[a]	1.82[a]	0.81[a]
0.5x	3.78[a]	2.11[a]	1.11[a]
1x	3.33[a]	2.00[a]	1.01[a]
2x	6.26[b]	3.71[b]	2.37[b]
5x	7.24[b]	4.02[b]	3.48[c]

Means followed by the same letters do not differ statistically (ANOVA, Tukey, p<0.05).

These results indicate that compound **3** induced cytogenetic changes at the 2x and 5x concentrations, whereas no statistically significant differences were observed between the lower concentrations (1x, 0.5x, and 0.2x) and the negative control (distilled water). The concentrations tested in the assay were based on the IC_{50} obtained in the acetylcholinesterase inhibition test for compound **3** (0.21 mM). For convenience, we refer to the concentrations as 0.2x (0.042 mM), 0.5x (0.105 mM), 1x (0.21 mM), 2x (0.42 mM) and 5x (1.05 mM).

Docking analyses

Docking simulation of the FDA approved drugs: The co-crystalized poses for the three ligands used as benchmarking were satisfactorily reproduced by the docking protocol (**Fig. S2**). The Root Mean Square Deviation (RMSD in Å) was 0.721 (E20), 0.720 (GNT) and 0.696 (HUP) and all-important ligand-enzyme contacts are predicted in the simulation (**Fig. S3**). It is important to emphasize that the docking protocol was independent of the reference X-ray structure (re-docking was not used here), therefore, the good agreement between predicted and experimental structures supports the docking protocol.

Table 5 shows the docking results for all compounds analyzed, including the main hydrophobic, polar (C…H-bond) and conventional H-bond contacts, in addition to the calculated drug-receptor affinity. Among the FDA approved drugs, the E20 has the greatest affinity (-10.1 kcal mol^{-1}) and is a strong AChE inhibitor. It binds to AChE site gorge with the benzyl ring directed to the catalytic anionic site (CAS) and stacking to Trp86 residue of the anionic domain (see **Fig. S4** for the definition of the main AChE binding site domains). The indanone ring is positioned near the peripherical anionic site (PAS), engaging in π-π stacking with Trp286 and forming H-bond with Phe295 of the acyl pocket. Additionally, the piperidine ring is in close contact with Tyr124, Phe338 and Tyr341 residues (**Fig. S3a**).

Table 5: The main ligand-receptor interactions obtained from docking simulation.

	Hydrophobic	Polar	H-bond	Affinity / kcal mol^{-1}
FDA approved drugs				
E20	Trp86, Tyr124, Phe338, Tyr341, Trp286	Tyr72, Val294, Tyr337	Phe295	-10.1
HUP	Trp86, Phe297, His447, Tyr449	Val126	Tyr133, Tyr337	-9.0
GNT	Trp86, Gly121, Phe295, Phe297, Phe338, His447	Asp74, Gly122, Tyr124, Ser125	Ser203	-7.8
RIS	Trp286, Phe297, Phe338, Tyr341		Tyr124, Tyr337	-7.3
Compounds 1-7 AChE inhibitors				
1	Trp86, His447		Asp74, Tyr124, Ser125, Tyr337, Tyr341	-7.4
2	Trp86, His447		Asp74, Thr83, Tyr124, Ser125, Tyr337, Tyr341	-7.6
3	His447	Trp86	Gln71, Tyr72, Asn87, Tyr124, Ser125	-7.5
4	Trp286	Tyr124	Ser293	-6.4
5	Trp86, His447	Ser125	Tyr72, Asp74, Asn87, Tyr124,	-7.2
6	Trp86, His447		Tyr337, Tyr341	-7.4
7	His447	Trp86, Tyr124, Ser125, Thr83, Tyr337	Asn87	-7.4

The 2D representations of the drug-receptor interactions are shown in Figure S3.

The HUP ligand also binds favorably to the AChE active site (-9.0 kcal mol^{-1}, **Fig. S3b**). Although smaller than E20, it possesses a significant molecular volume that favors interactions deep within the binding gorge. The main anchor points are located in the anionic domain, with two H-bonds formed with Tyr133 and Tyr337. Additionally, hydrophobic interactions are observed at the CAS domain, involving Phe297 and Tyr449.

GNT also binds at the CAS (-7.8 kcal mol^{-1}), forming a H-bond between Ser203 and the benzofuran moiety. In addition, several hydrophobic interactions are predicted with His447 (CAS domain); Trp86 and Phe338 (anionic domain); and Phe295 and Phe297 (acyl pocket) (**Fig. S3c**).

The RIS compound showed the lowest affinity for AChE (-7.3 kcal mol^{-1}). It binds with the *N*-ethyl-*N*-methylcarbamate group oriented toward the CAS domain, while H-bonds with Tyr124 (PAS domain) and Tyr337 (anionic site) stabilize the molecule near the PAS domain (**Fig. S5**). Additionally, hydrophobic interactions observed between the dimethylamino group and PAS residues (Trp286 and Tyr341).

Docking simulation of the adamantane derivatives: The compounds **1-7** proposed here have an adamantane group attached to amine derivatives (**Fig. 1**). All seven molecules showed similar affinities, from -6.4 to -7.6 kcal mol^{-1}, and

comparable binding modes (Table 5), with the adamantane group engaging in hydrophobic interactions with Trp86 and His447 in the anionic site (CAS domain). The terminal amino group is oriented toward the PAS domain, forming H-bonds with several residues, primarily tyrosinases in the region - Tyr124, Tyr337, and Tyr341. Analysis of **Fig. 2a** and **2b** reveals that **1** and **2** adopt similar conformations within the binding site, with the adamantane ring interacting with Trp86 and His447 in the CAS domain, while the terminal amine forms hydrogen bonds with Tyr337 and His341 in the PAS domain. In the case of compound **3**, which contains a butyl C-chain, the folded conformation is not predicted (**Fig. 2c**), and the terminal amine group forms short contacts with Gln71 and Tyr72 in the PAS domain. Analysis of the binding affinities presented in the last column of Table 5 reveals very similar values for ethyl (compound **1**: -7.4 kcal mol^{-1}), propyl (**2**: -7.6 kcal mol^{-1}) and butyl (**3**: -7.5 kcal mol^{-1}) derivatives. The compounds **4**, **5** and **6** were derived from **1** with an ethyl C-chain. The alkylation of the terminal amine (compound **4**) changes and weakens the binding mode, with the adamantane group directed to the PAS domain. Two important drug-receptor contacts were observed with Trp286 (PAS domain) and Ser293 (Acyl pocket) (**Fig. 2d**). The loss of H-bonds with Tyr in the PAS domain resulted in an affinity of only -6.4 kcal mol^{-1} for **4**, the lowest among all molecules screened (see Table 5). The compounds **5** and **6** bind similarly to **1**; however, the change of the -NH group to -S in **5** decreased the affinity to -7.2 kcal mol^{-1} due to loss of H-bond to Tyr337 (**Fig. 2e**). On the other hand, replacing the terminal -NH_2 group with an -OH group (compound **6**) did not affect the binding mode or even the affinity, maintaining the four essential anchor points Trp86, His447 (near the CAS domain) and Tyr337, Tyr341 (near the PAS domain) (**Fig. 2f**). Lastly, compound **7** was analyzed, which presents a hydro-pyrazine ring. The binding mode and affinity is like **1**, but the H-bonds are less frequent (**Fig. 2g**), which might support the importance of the free terminal amine for these compounds observed experimentally.

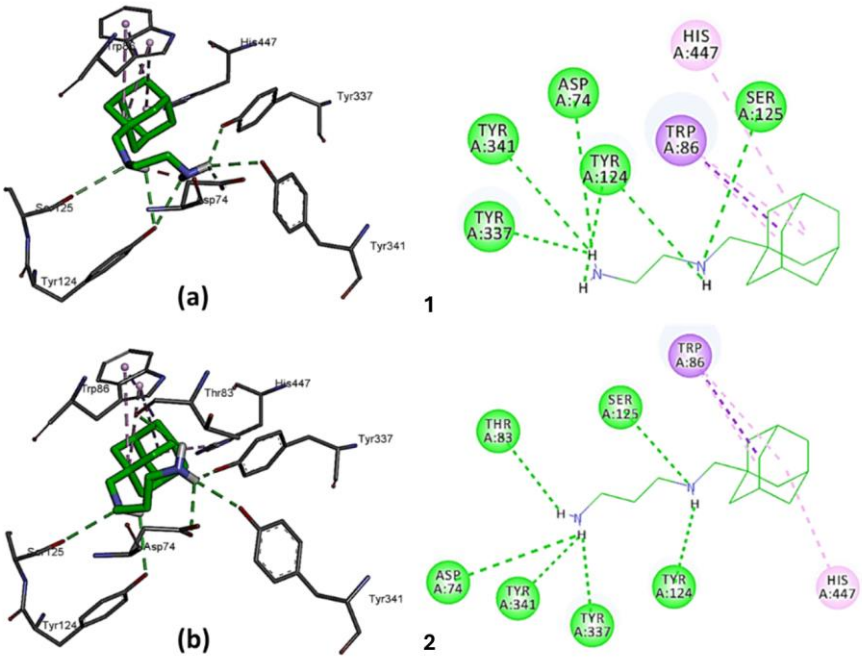

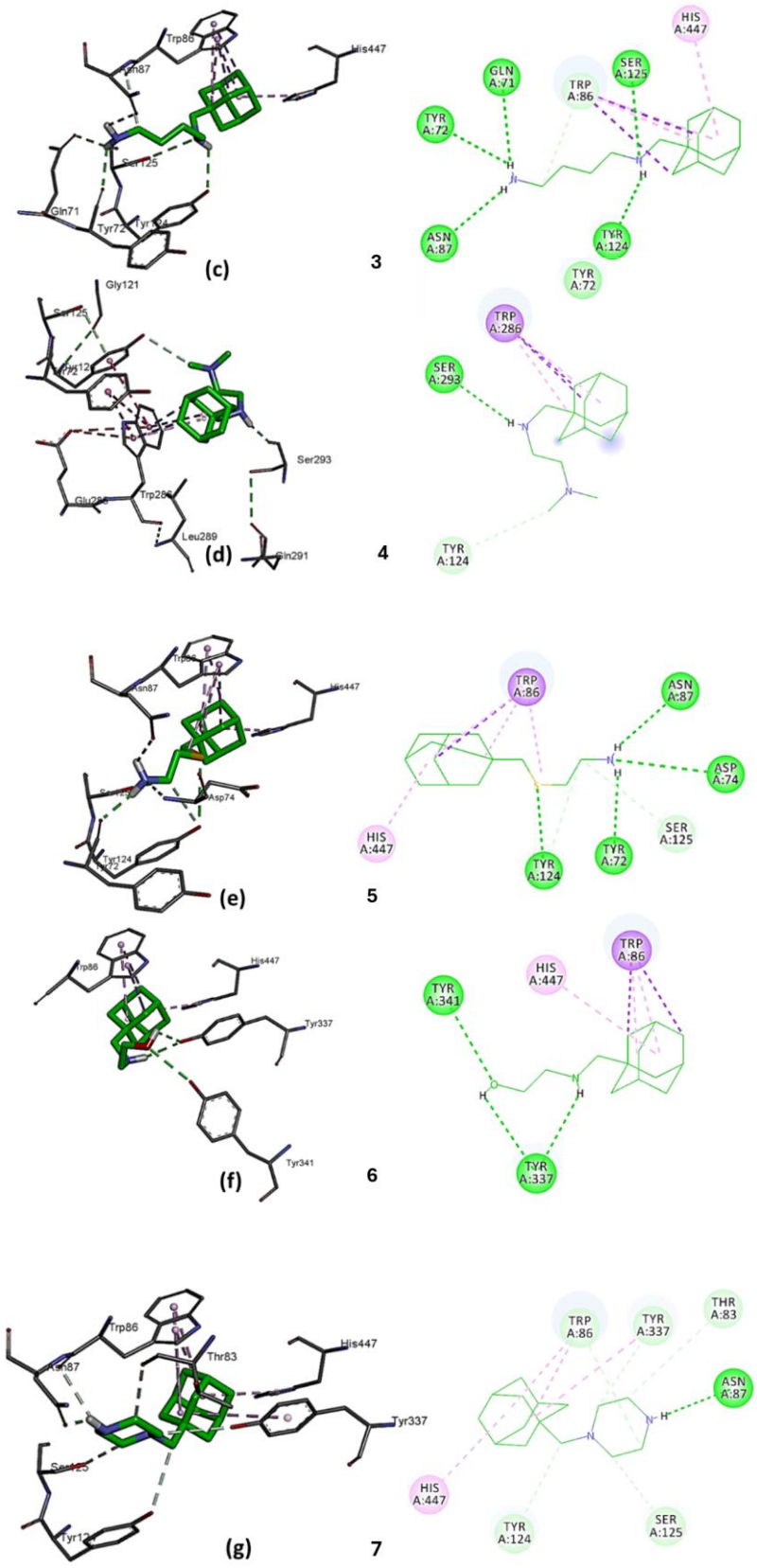

Fig. 2: Compounds 1-7…AChE binding mode.

In summary, docking analysis of the seven compounds synthetized here indicates that **2** and **3** exhibits the key features of a potential AChE inhibitor: (i) an adamantane hydrophobic group moiety interacting with Trp86 and His447 (CAS domain), and (ii) an alkyl diamine chain forming H-bonds with PAS residues, mainly, Tyr337 and Tyr441. Among the series, compounds **2** and **3** showed the highest affinities (-7.6 and -7.5 kcal mol^{-1}), both comparable to GNT (-7.8 kcal mol^{-1}), but lower than FDA-approved drugs: E20 (-10.1 kcal mol^{-1}) and HUP (-9.0 kcal mol^{-1}).

In vivo* studies with *C. elegans

C. elegans offers unique perspectives as a neurotoxicological model. Some simple behavioral assays, such as locomotion, pharyngeal pumping, and touch response, can provide insights into neuronal system functioning and detect abnormalities. Alterations in locomotive behaviors afford a rapid and sensitive indicator for evaluating nervous system damage.[27] The exposure to different concentrations of compound **3** for 48 h did not significantly affect the survival of *C. elegans* compared to the control group. However, memantine exposure induced a significant decrease in the number of live nematodes at concentrations of 50 µM (87.7%, $p < 0.05$) and 100 µM (83.0%, $p < 0.005$). Due to this toxicity, subsequent tests will use the 25 µM concentration for all materials. Body length was affected by both substances, compound **3** ($p < 0.05$) and memantine ($p < 0.005$).

In *C. elegans*, the pharyngeal neuromuscular innervation consists of a subset of cholinergic and glutamatergic neurons that synapse onto the radial muscles of the pharynx. The elimination of cholinergic signaling leads to a complete loss of pumping, and the presence of anti-cholinergic substances in high doses can cause cholinergic hyperstimulation, resulting in pharyngeal hypercontraction.[28,29] Worms treated with compound **3** had a significant increase in pharyngeal pumping (43.5/10 s, $p < 0.001$) compared to the control group (33.2/10 s) and memanine (33.8/10 s). This could be related to an increase in cholinergic activity provided by compound **3** (more ACh available through AChE inhibition) in a dose-dependent manner. The concentration used (25 µM) was able to stimulate the muscle contraction, but was not high enough to induce hyperstimulation and paralysis of the pharyngeal muscle. *C. elegans* did not experience a change in touch response after being exposed to memantine, but nematodes exposed to compound **3** had a reduction in response to touch ($p < 0.05$) compared to the control group. In the nematode, ASH sensory neurons regulate the response to sensory stimuli through glutamate acting on the ionotropic non-NMDA glutamate receptor - GLR-1.[30]

Our findings suggest that compound **3** affects mechanosensation by interfering with glutamatergic neurotransmission, influencing the ASH neurons or the signaling pathways they control. Memantine acts as a non-competitive voltage-dependent antagonist on activated NMDA receptors, blocking their ionic channel and therefore, showing no significant difference in the touch response test compared to the control group.

Analyzing the locomotion activity parameters of nematodes exposed to compound **3** and memantine, we observed a significant increase in the head thrashes, swimming speed, and wave initiation rate for both treatments. As shown in **Fig 3**, both substances increased the number of head thrashes when compared to the control group (Compound **3** 24.0%, $p<0.01$; and Mem. 28.1%, $p<0.001$). In the control group, the number of thrashes was 149 ± 29.2, while in groups with compound **3** and memantine, it was 185 ± 13.7 and 191 ± 15.6 thrashes per minute, respectively. In mutant Worms (CL2006), memantine showed no significant difference between treated and control worms. This strain expresses human Aβ in muscle cells, accumulating in intracellular cytoplasmic deposits [31]. Compound **3** showed an increase in head trash when compared to the control group (CL2006). In the control group, the number of thrashes was 37.2 ± 14.3, while in compound **3,** it was 72 ± 21.9. This improvement (93.5%) in movement may be related to the

multitargeting ability of compound **3**, modulating the cholinergic pathway. In wave initiation rate and swimming speed, we observe an increase in movement in both substances when compared to the wild-type *C. elegans* strain (N2). For the control group, the rate of swimming speed was 262.6 ± 79.9 µm/s. Compound **3** showed an increase of 19.6% (314.0 ± 80.2 µm/s; $p < 0.01$), and memantine showed a 33.9% increase (351.6 ± 73.3 µm/s; $p < 0.0001$). Another neurotransmitter related to locomotor activity in *C. elegans* is glutamate, which acts on NMR-1 (an NMDA-type ionotropic glutamate receptor subunit) expressed in the interneurons of the locomotor control circuit. Brockie and coworkers have demonstrated that mutants with deletion of nmr-1 disrupt the pattern of locomotion, increasing the mean duration of forward movement when compared to wild-type worms [30], [32]. Even with the diversity of neurotransmitters and receptors involved in the motor activity of *C. elegans*, characterized by distinguishable neural networks, the data showed that compound **3** exhibited activity similar to memantine in locomotor parameter tests for the wild-type strain.

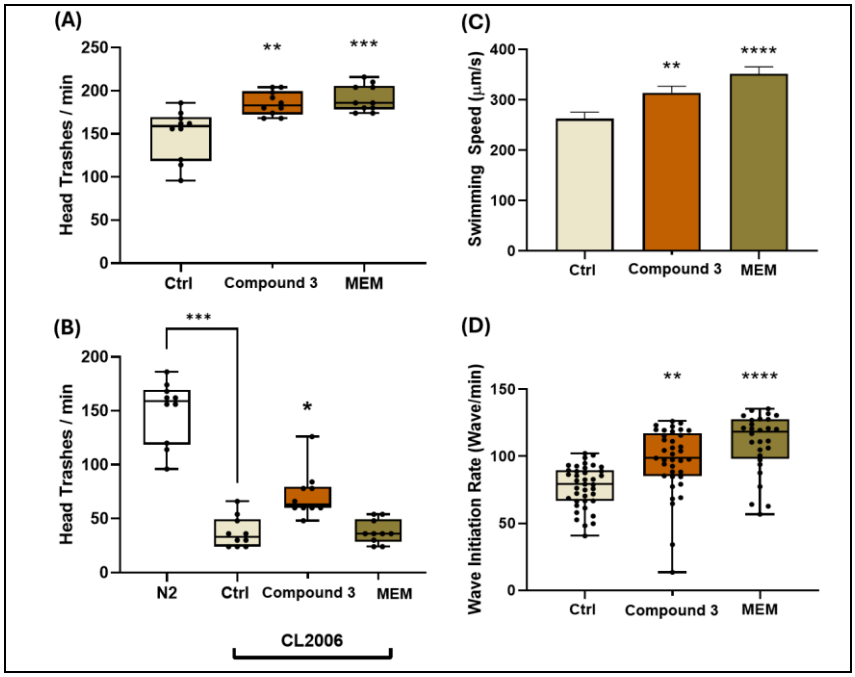

Fig. 3: Effects of compound 3 treatment and memantine (MEM) on locomotor activity parameters in *C. elegans*.

*(A) Head thrashes in wild-type N2 worms. (B) Head thrashes in transgenic CL2006 strain. (C) Swimming speed (µm/s). (D) Wave initiation rate (waves/min). N=30 worms per group. The analysis was performed using WormLab software. Statistical analyses were performed using One-Way ANOVA followed by Tukey's post hoc test or Kruskal–Wallis followed by Dunn's multiple comparisons test when normality (Shapiro-Wilk) was not satisfied. Asterisks indicate significant differences compared to the control group (*p<0.05; **p<0.01; ***p<0.001; ****p<0.0001). Ctrl: control group.*

CONCLUSIONS

Adamantane-derived compounds could be considered as potential multi-targeted drugs for Alzheimer's disease. Our results demonstrate the ability of these compounds, especially compound **3**, to act as iAChEs *in vitro* and *in vivo*. This molecule also modulates *C. elegans* locomotor parameters similarly to memantine, and these findings are consistent with the molecule's intended purpose; the adamantane moiety acts on glutamate receptors, and the amine moiety acts on

acetylcholinesterase, as demonstrated in the computational analysis. Further studies are needed to clarify the actions of these molecules *in vivo*, including the use of more complex models of Alzheimer's disease.

SUPPLEMENTARY INFORMATION: Supplementary information is provided below references.

ACKNOWLEDGMENTS

The authors would like to thank the Federal University of Juiz de Fora, Fapemig and CNPq for financial support. HS thanks to CNPq (research grant number 314399/2023-2).

CONFLICT OF INTEREST

The authors declare that they have no conflict of interest.

REFERENCES

1. Q. Zheng and X. Wang, “Alzheimer’s disease: insights into pathology, molecular mechanisms, and therapy,” *Protein Cell*, Feb. 2024. doi: 10.1093/procel/pwae026.
2. M. Agarwal, M. R. Alam, M. K. Haider, M. Z. Malik, and D. K. Kim, “Alzheimer’s disease: An overview of major hypotheses and therapeutic options in nanotechnology,” *Nanomaterials*, Jan. 2021; 11(1): 1–18, , doi: 10.3390/nano11010059.
3. S. V Rekha, F. C. Rinsi P, F. Rinciya, L. K. Balkkees V, and M. A. Sinan K, “A SYSTEMATIC REVIEW OF Azadirachta indica FOR THE DEVELOPMENT OF AN IN-VITRO MODEL FOCUSING ON ALZHEIMER’S DISEASE,” *World Journal of Pharmaceutical Science and Research*, 2026; 5(4): 253–266. doi: 10.5281/zenodo.19333382.
4. U. Soni, K. Singh, D. Jain, and R. Pujari, “Exploring Alzheimer’s disease treatment: Established therapies and novel strategies for future care,” Jul. 05, 2025, *Elsevier B.V.* doi: 10.1016/j.ejphar.2025.177520.
5. G. G. Gaykee, S. J. Tamboli, and P. N. Sawant Pune, “Role of herbal transdermal patches in Alzheimer’s disease,” *World Journal of Pharmaceutical Science and Research*, Apr. 2026; 5(4): 267–284, , doi: 10.5281/zenodo.19335248.
6. G. Livingston *et al.*, “Dementia prevention, intervention, and care: 2024 report of the Lancet standing Commission,” Aug. 10, 2024, *Elsevier B.V.* doi: 10.1016/S0140-6736(24)01296-0.
7. C. Pathak and U. D. Kabra, “A comprehensive review of multi-target directed ligands in the treatment of Alzheimer’s disease,” Mar. 01, 2024, *Academic Press Inc.* doi: 10.1016/j.bioorg.2024.107152.
8. T. Sajed *et al.*, “Accurate prediction of H NMR chemical shifts os small molecules using machine learning,” *Metabolites*, May 2024; 14: p. 290.
9. P. J. Garegg and B. Samuelsson, “Novel reagent system for converting a hydroxy-group into an iodo-group in carbohydrates with inversion of configuration,” *J Chem Soci, Chem Commun*, 1979; 22: pp. 978–980.
10. G. Barbosa, “Síntese de derivados adamantóides diaminados e amino álcoois, potenciais agentes farmacológicos,” UFJF, Juiz de Fora, 2014.
11. G. L. Ellman, K. D. Courtney, V. Andres, and R. M. Featherstone, “A new and rapid colorimetric determination of acetylcholinesterase activity,” Pergamon Press Ltd, 1961.
12. N. Sreejayan and M. N. Rao, “Free radical scavenging activity of curcuminoids. ,” *Arzneimittelforschung*, 1996; 46(2): 169–171.

13. T. Mosmann, “Rapid Colorimetric Assay for Cellular Growth and Survival: Application to Proliferation and Cytotoxicity Assays,” 1983.
14. B. N. Meyer, N. A. Ferrigni, J. E. Putnam, L. B. Jacobsen, D. E. Nichols, and J. L. Mclaughlin, “Brine Shrimp: A Convenient General Bioassay for Active Plant Constituents,” Jan. 1982.
15. D. J. Finney, “The adjustment for a natural response rate in probit analysis,” *Annals of Applied Biology*, 1949; 36(2): 187–195. doi: 10.1111/j.1744-7348.1949.tb06408.x.
16. P. Burchardt *et al.*, “Cytological and genome size data analyzed in a phylogenetic frame: Evolutionary implications concerning sisyrinchium taxa (Iridaceae: Iridoideae),” *Genet. Mol. Biol.*, 2018; 41(1): 288–307. doi: 10.1590/1678-4685-gmb-2017-0077.
17. M. J. Frisch *et al.*, “Gaussian 09,” 2010, *Gaussian Inc., Wallingford.*: Revision B.01.
18. L. Gorecki *et al.*, “Rational design, synthesis, and evaluation of uncharged, ‘smart’ bis-oxime antidotes of organophosphate-inhibited human acetylcholinesterase,” *Journal of Biological Chemistry*, Mar. 2020; 295(13): 4079–4092. doi: 10.1074/jbc.RA119.012400.
19. O. Trott and A. J. Olson, “AutoDock Vina: Improving the speed and accuracy of docking with a new scoring function, efficient optimization, and multithreading,” *J. Comput. Chem.*, Jan. 2010; 31(2): 455–461. doi: 10.1002/jcc.21334.
20. J. Eberhardt, D. Santos-Martins, A. F. Tillack, and S. Forli, “AutoDock Vina 1.2.0: New Docking Methods, Expanded Force Field, and Python Bindings,” *J. Chem. Inf. Model.*, Aug. 2021; 61(8): 3891–3898. doi: 10.1021/acs.jcim.1c00203.
21. J. Cheung *et al.*, “Structures of human acetylcholinesterase in complex with pharmacologically important ligands,” *J. Med. Chem.*, Nov. 2012; 55(22): 10282–10286. doi: 10.1021/jm300871x.
22. M. Porta-de-la-Riva, L. Fontrodona, A. Villanueva, and J. Cerón, “Basic Caenorhabditis elegans Methods - Synchronization and Observation,” *J. Vis. Exp.*, Jun. 2012, doi: 10.3791/4019.
23. F. da Silva *et al.*, “JM-20 affects GABA neurotransmission in Caenorhabditis elegans,” *Neurotoxicology*, Dec. 2022; 93: 37–44. doi: 10.1016/j.neuro.2022.08.012.
24. T. L. da Silveira *et al.*, “Caenorhabditis elegans as a model for studies on quinolinic acid-induced NMDAR-dependent glutamatergic disorders,” *Brain Res. Bull.*, Oct. 2021; 175: pp. 90–98. doi: 10.1016/j.brainresbull.2021.07.007.
25. B. Vinutha *et al.*, “Screening of selected Indian medicinal plants for acetylcholinesterase inhibitory activity,” *J. Ethnopharmacol.*, Jan. 2007; 109(2): 359–363. doi: 10.1016/j.jep.2006.06.014.
26. V. Shukla, S. K. Mishra, and H. C. Pant, “Oxidative stress in neurodegeneration,” *Adv. Pharmacol. Sci.*, vol. 2011, 2011, doi: 10.1155/2011/572634.
27. A. Adedara *et al.*, “Versatility of Caenorhabditis elegans as a Model Organism for Evaluating Foodborne Neurotoxins and Food Bioactive Compounds in Nutritional Neuroscience,” Jun. 01, 2025, *Springer*. doi: 10.1007/s12035-025-04705-y.
28. P. G. Izquierdo, V. O’Connor, A. C. Green, L. Holden-Dye, and J. E. H. Tattersall, “C. elegans pharyngeal pumping provides a whole organism bio-assay to investigate anti-cholinesterase intoxication and antidotes,” *Neurotoxicology*, Jan. 2021; 82: pp. 50–62. doi: 10.1016/j.neuro.2020.11.001.

29. N. F. Trojanowski, D. M. Raizen, and C. Fang-Yen, “Pharyngeal pumping in Caenorhabditis elegans depends on tonic and phasic signaling from the nervous system,” Mar. 2016. [Online]. Available: www.nature.com/scientificreports/
30. J. Paltian *et al.*, “7-chloro-4-(phenylselanyl) quinoline incorporation into polymeric nanocapsules improves its pharmacological action: Physicochemical, toxicological, and behavioral studies,” *Int. J. Pharm.*, Mar. 2025; vol. 673. doi: 10.1016/j.ijpharm.2025.125370.
31. C. D. Link, “Expression of human f8-amyloid peptide in transgenic Caenorhabditis elegans,” 1995. [Online]. Available: https://www.pnas.org
32. P. J. Brockie, J. E. Mellem, T. Hills, D. M. Madsen, and A. V Maricq, “The C. elegans Glutamate Receptor Subunit NMR-1 Is Required for Slow NMDA-Activated Currents that Regulate Reversal Frequency during Locomotion,” 2001.

SUPPLEMENTARY MATERIALS

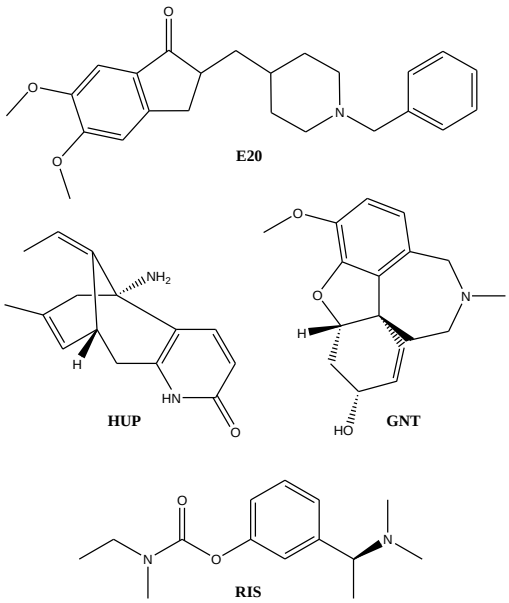

Fig. S1: Structures of the FDA approved AChE inhibitors: donepezil (E20), (-)galantamine (GNT), (-)huperzine A (HUP) and rivastigmine (RIS).

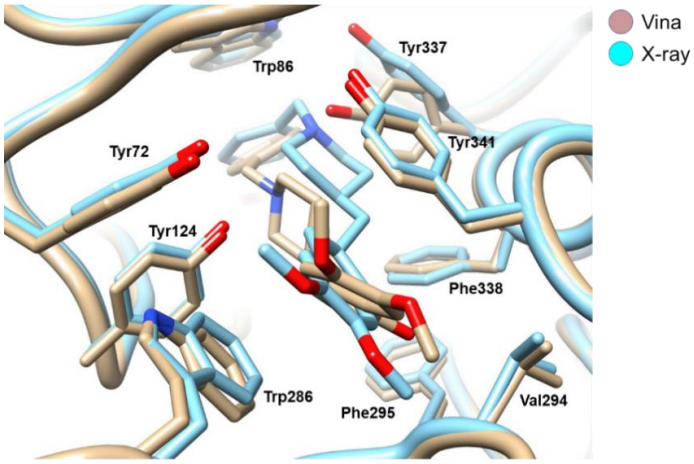

(a) E20 (4EY7) – RMSD = 0.721 Å

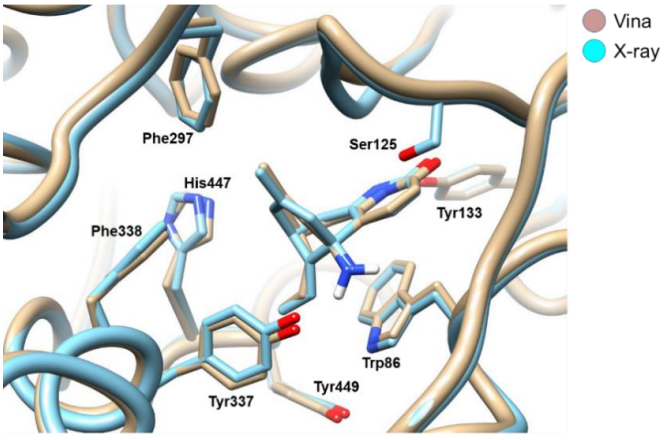

(b) HUP (4EY5) – RMSD = 0.696 Å

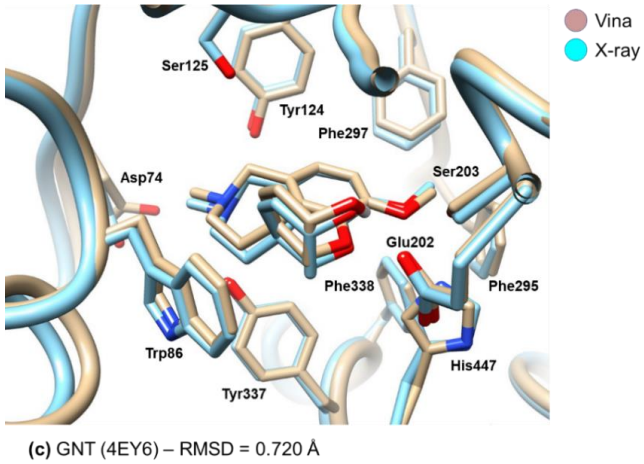

Fig. S2: Overlap of the X-ray and docked (Vina) structures for the FDA approved drugs. The PDB code is shown in parenthesis and the RMSD using all residues is provided.

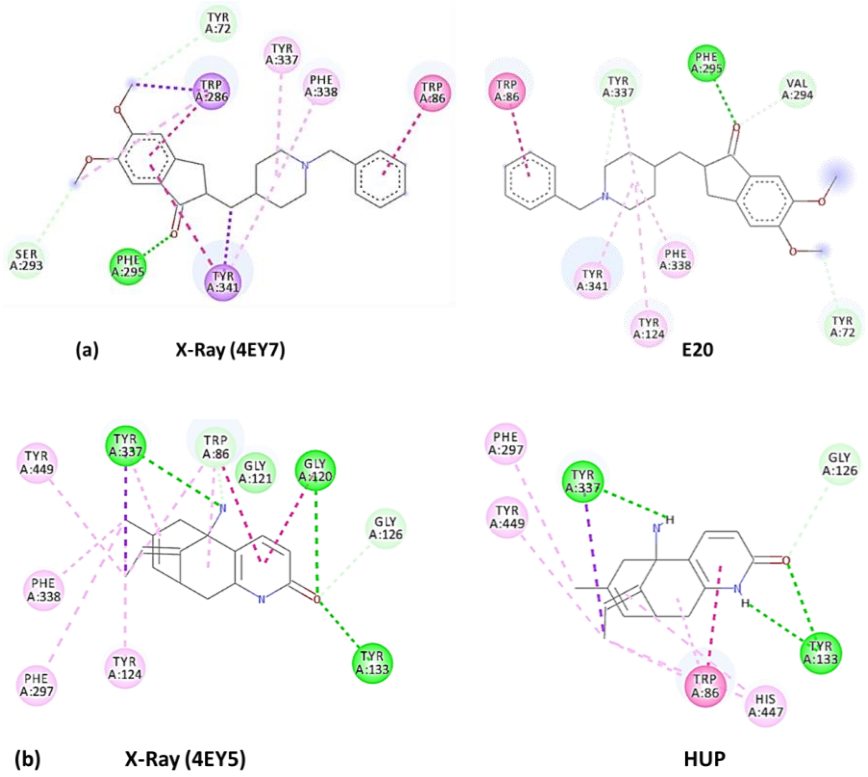

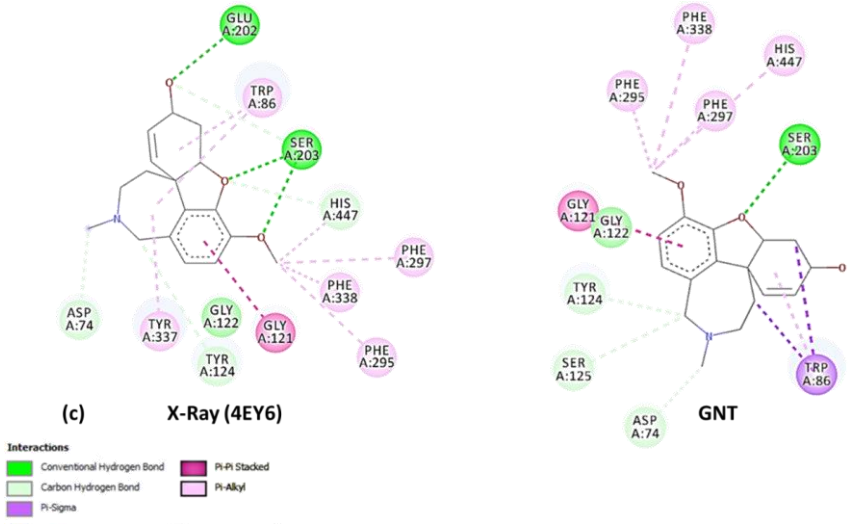

Fig. S3: 2D representations of the drug-receptor interactions for FDA approved drugs, highlighting key H-bonds, hydrophobic contacts, and π-π stacking interactions within the active site.

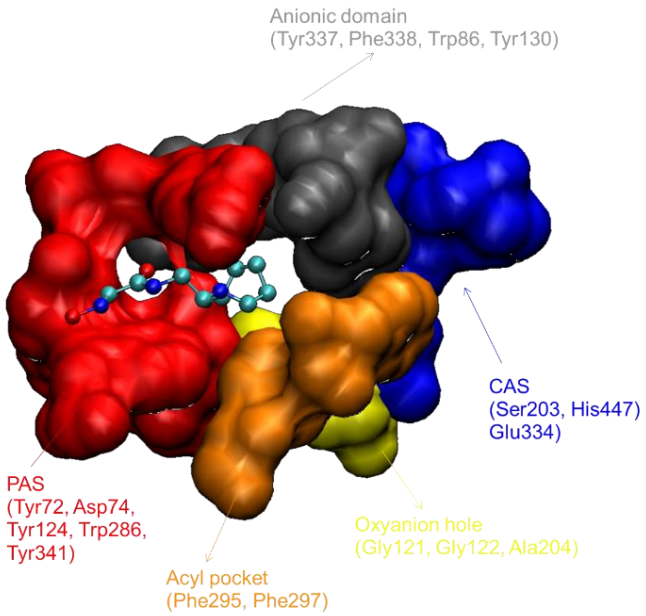

Fig. S4: AchE binding site. The PDB 6U37 structure was used with the PVQ co-crystalized ligand.

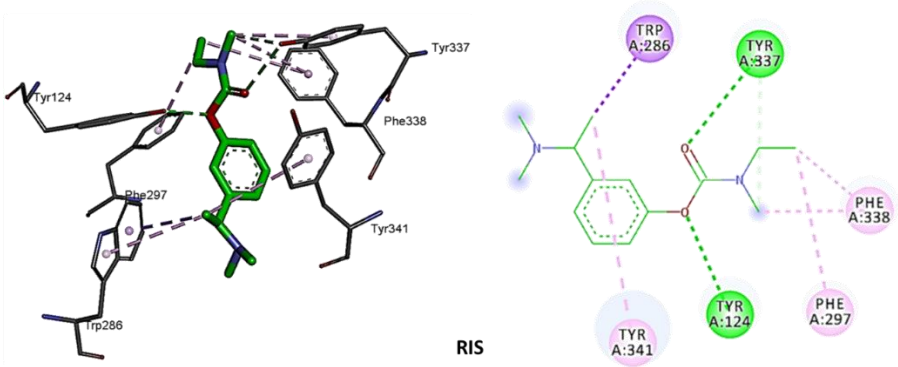

Fig. S5: Rivastigmine (RIS) AChE binding mode.